Dendrochronologia 69 (2021) 125879

Contents lists available at ScienceDirect

Dendrochronologia

journal homepage: www.elsevier.com/locate/dendro

ORIGINAL ARTICLE

A lonely dot on the map: Exploring the climate signal in tree-ring density and stable isotopes of clanwilliam cedar, South Africa

Tom De Mil [a,b,c,d,*,1], Matthew Meko [a], Soumaya Belmecheri [a], Edmund February [e], Matthew Therrell [f], Jan Van den Bulcke [b,c], Valerie Trouet [a]

[a] Laboratory of Tree-Ring Research, University of Arizona, 1215 E Lowell St, Tucson, AZ, 85721, United States
[b] UGent-Woodlab, Laboratory of Wood Technology, Department of Environment, Ghent University, Coupure Links 653, B-9000, Gent, Belgium
[c] Ghent University Centre for X-ray Tomography (UGCT), Proeftuinstraat 86, B-9000, Gent, Belgium
[d] Forest Is Life, TERRA Teaching and Research Centre, Gembloux Agro Bio-Tech, University of Liège, Passage des Déportés 2, B-5030, Gembloux, Belgium
[e] Department of Biological Sciences, University of Cape Town, HW Pearson Building, University Ave N, Rondebosch, Cape Town, 7701, South Africa
[f] Department of Geography, University of Alabama, Box 870322, Tuscaloosa, AL, 35401, United States

ARTICLE INFO

Keywords:
Minimum density (MND)
Maximum latewood density (MXD)
Maximum latewood blue intensity (MXBI)
Stable isotopes
South Africa
Widdringtonia cedarbergensis
X-ray Computed micro tomography (X-ray CT)

ABSTRACT

Clanwilliam cedar (*Widdringtonia cedarbergensis*; WICE), a long-lived conifer with distinct tree rings in Cape Province, South Africa, has potential to provide a unique high-resolution climate proxy for southern Africa. However, the climate signal in WICE tree-ring width (TRW) is weak and the dendroclimatic potential of other WICE tree-ring parameters therefore needs to be explored. Here, we investigate the climatic signal in various tree-ring parameters, including TRW, Minimum Density (MND), Maximum Latewood Density (MXD), Maximum Latewood Blue Intensity (MXBI), and stable carbon and oxygen isotopes ($\delta^{18}O$ and $\delta^{13}C$) measured in WICE samples collected in 1978. MND was negatively influenced by early spring (October-November) precipitation whereas TRW was positively influenced by spring November-December precipitation. MXD was negatively influenced by autumn (April-May) temperature whereas MXBI was not influenced by temperature. Both MXD and MXBI were negatively influenced by January-March and January-May precipitation respectively. We did not find a significant climate signal in either of the stable isotope time series, which were measured on a limited number of samples. WICE can live to be at least 356 years old and the current TRW chronology extends back to 1564 CE. The development of full-length chronologies of alternative tree-ring parameters, particularly MND, would allow for an annually resolved, multi-century spring precipitation reconstruction for this region in southern Africa, where vulnerability to future climate change is high.

1. Introduction

Reliable instrumental climate measurements are only available globally for approximately the past century (Jones et al., 2009). Climate proxies that provide longer time series are therefore needed to put current and projected anthropogenic climate change in a longer-term perspective (Kaufman et al., 2020). Tree-ring data, primarily based on tree-ring width (TRW) measurements, are one of the most widely used and geographically distributed high-resolution climate proxies to study the climate of the Common Era (Ahmed et al., 2013; Büntgen et al., 2011). In addition to TRW, many other tree-ring parameters offer potential for quantitative climate reconstruction. In the Northern Hemisphere (NH), Maximum Latewood Density (MXD) is a reliable proxy for summer temperature (Anchukaitis et al., 2017; Klippel et al., 2019; St. George and Esper, 2018; Trouet et al., 2012), because it reflects the cell-wall thickness of latewood cells that is positively influenced by temperature at higher latitudes (Rathgeber, 2017). Minimum density (MND), on the other hand, often occurs early in the growing season and is negatively impacted by moisture (Camarero et al., 2014, 2017) because of its hydraulic-functional response to climate, with wider lumina corresponding to lower density in the earlywood (Björklund et al., 2017). Both MXD and MND can be measured using X-ray densitometry, which is a labor-intensive and time-consuming method (Schweingruber, 1988). As an alternative method, Maximum Latewood

* Corresponding author. Present address at: Coupure Links 653, B-9000, Gent, Belgium.
E-mail address: Tom.demil@uliege.be (T. De Mil).
[1] Present address: Passage des Déportés 2, B-5030 Gembloux, Belgium.

https://doi.org/10.1016/j.dendro.2021.125879
Received 16 November 2020; Received in revised form 4 June 2021; Accepted 30 August 2021
Available online 31 August 2021

Blue Intensity (MXBI) (Björklund et al., 2014; Campbell et al., 2011; Rydval et al., 2014) requires no advanced equipment, but the reliability of MXBI data as climate proxies depends on surface treatment and their skill in capturing low-frequency climate trends is debated (see (Björklund et al., 2019)). Recent advances in X-ray Computed micro tomography (X-ray CT) for tree cores (De Mil et al., 2016) also provide reliable density estimates without sample preparation (Björklund et al., 2019; Van den Bulcke et al., 2014). In addition to these methods, the quantitative measurement of wood anatomical traits has recently shown great potential as a high-resolution climate proxy (De Mil et al., 2019; Fichtler and Worbes, 2012; Olano et al., 2013; Pritzkow et al., 2016). Finally, carbon ($\delta^{13}C$) and oxygen ($\delta^{18}O$) stable isotope measurements have also successfully been used for the development of century-long precipitation reconstructions (McCarroll and Loader, 2004; Treydte et al., 2006; Andreu-Hayles et al., 2017).

Most tree-ring chronologies (predominantly TRW) available in the International Tree-Ring Database (ITRDB) (National Climate Data Center, 2011) are located in the NH, whereas climate-sensitive, annually resolved tree-ring data are less available in the Southern Hemisphere (SH), where there is less land mass. Moreover, only few of the above-mentioned tree-ring parameters, other than TRW, have been examined in the SH, with the exception of density and cellular parameters in Australia & New Zealand (e.g. Allen et al., 2012, 2019,2018; Blake et al., 2020; Drew et al., 2013; O'Donnell et al., 2016) and stable isotopes in South America (e.g. Lavergne et al., 2017; Roig et al., 2006) and in Central Africa (Colombaroli et al., 2016).

In southern Africa, paleoclimate proxies include only a limited number of tree-ring records (but see e;g; Therrell et al., 2006; Trouet et al., 2010; Woodborne et al., 2018; Ngoma et al., 2017), but other annual-resolution records include documentary records, such as missionary correspondence (Endfield and Nash, 2002) and shiplog records (Hannaford et al., 2015; Nicholson et al., 2012), and lower-resolution proxies that include diatom records (Stager et al., 2012), hyrax middens, sediment cores, speleothems, pollen, and micro-charcoal records (e.g. Chase et al., 2015; Scott et al., 2021; Tyson et al., 2002; Valsecchi et al., 2013). In South Africa, only one crossdated TRW record (1564–1977 CE) has been developed, based on clanwilliam cedar (*Widdringtonia cedarbergensis*; WICE) from the "Die Bos" site in the Cedarberg mountains (Dunwiddie and LaMarche, 1980), where also pooled $\delta^{13}C$ records were measured on the same trees (February and Stock, 1999).

The climate in this southwestern South Africa region is Mediterranean, with wet and cool winters (April to September) and dry and warm summers (October to March) and is classified as a winter rainfall zone (Chase and Meadows, 2007; Neukom et al., 2014). The winter rainfall zone is projected to be prone to future droughts and rising temperatures, with negative effects on agriculture and livelihoods (Archer et al., 2019).

Woody growth in WICE was estimated to occur from October to March (Dunwiddie and LaMarche, 1980), but radial stem growth occurs also from February to June, at the start of the wet winter (February et al., 2007) and it is shown that the trees show intra-annual bands or unclear ring boundaries which complicates dating on a significant portion of the samples (February and Stock, 1998).

Other species of the *Widdringtonia* genus have been explored for their tree-ring potential (February and Gagen, 2003), but have not been proven to crossdate well (Therrell et al., 2006). The climate signal is weak in both the WICE TRW record (Dunwiddie and LaMarche, 1980; Zucchini and Hiemstra, 1983) and the $\delta^{13}C$ record (February and Stock, 1999), which warrants the investigation of additional WICE tree-ring parameters.

Here we perform a multi-parameter dendroclimatic analysis including annual MND, TRW, MXD, MXBI, $\delta^{18}O$, and $\delta^{13}C$ measurements from WICE cores from the Die Bos collection (Dunwiddie and LaMarche, 1980). Our aim is to explore the strength of precipitation and temperature signals in these various tree-ring parameters. We focus particularly on density parameters (MND and MXD), which offer great potential for high-resolution climate reconstruction in regions that were previously not considered suitable. We hypothesize that:

1 MND, TRW, $\delta^{18}O$, and $\delta^{13}C$ measurements contain a precipitation signal;
2 MXD and MXBI measurements contain a temperature signal.

Our multi-tree-ring parameter approach is aimed at investigating the potential of tree-ring data to reconstruct climate in the Mediterranean region of South Africa, which recently has experienced a strong multi-year rainfall deficit (Wolski et al., 2021).

2. Material and methods

2.1. Study area

The "Die Bos" site (-32.4 °S, 19.22 °E) is located in the Cedarberg mountain range in South Africa at an altitude of 1330 m above sea level (Zucchini and Hiemstra, 1983) (Fig. 1A). The site is in a winter rainfall zone with mean annual temperature of 16.6 °C and mean annual precipitation of 355 mm. The majority of the annual precipitation falls in the winter months (May-August; Fig. 1B). The site is part of the fynbos biome (February et al., 2007) and the trees grow on rocky substrate.

2.2. Tree-ring samples

For the X-ray CT measurements (MXD and MND), we selected 20 WICE cores from 10 trees collected at the "Die Bos" site in March 1978 (Dunwiddie and LaMarche, 1980). These samples are archived in the University of Arizona Laboratory of Tree-Ring Research (LTRR). We based our selection of samples from the collection on the interseries correlation of the original (55) dated TRW series (Dunwiddie and LaMarche, 1980).

As shown above, the growing season is from October to March (Dunwiddie and LaMarche, 1980) but recent intra-annual diameter measurements have shown growth from February to June (February et al., 2007). Cambial growing season of conifers at extratropical latitudes (such as Die Bos) is primarily defined by daylength and photoperiod (e.g. Morino et al., 2021; Polgar and Primack, 2011). The cambial growing season of trees in similar SH Mediterranean climates (e.g. Mundo et al., 2010) is defined from approximately October until April and thus similar to the definition of our growing season. The actual growing season could potentially be longer than the October-March period. For instance, our samples were collected in March 1978 and the latewood of the most recent 1977–1978 ring was not fully formed yet (Figs. 2B, S1). This suggests that in March, the growing season was ending (latewood formed), but that the trees were not dormant yet. In addition, unclear tree-ring boundaries and intra-annual bands (February and Stock, 1998) confirm that there could indeed be resumption of growth due to favourable conditions in late summer/fall.

To be conform with other paleoclimate reconstructions in southern Africa (e.g. Therrell et al., 2006), the Shulman shift (Schulman, 1956) was not applied, i.e. TRW values were assigned to the year when the growing season (October-March) starts. For MXBI measurements, we selected a subset of 10 cores from 7 trees with the best sanding quality and fewest resin ducts to avoid artefacts. Stable carbon and oxygen isotopes were measured on another subset of 4 cores.

2.3. X-ray CT toolchain and blue intensity

The 20 samples were X-ray CT scanned while still mounted. To allow for this, we reduced the size of the sample holders by cutting the section that contained the core (Fig. 2A) in order to fit into the sample holder. We extracted the samples in a Soxhlet apparatus for 24 h in ethanol to remove resins and extractives. We then scanned samples at 10 μm with the HECTOR scanning system (Van den Bulcke et al., 2019), which is a

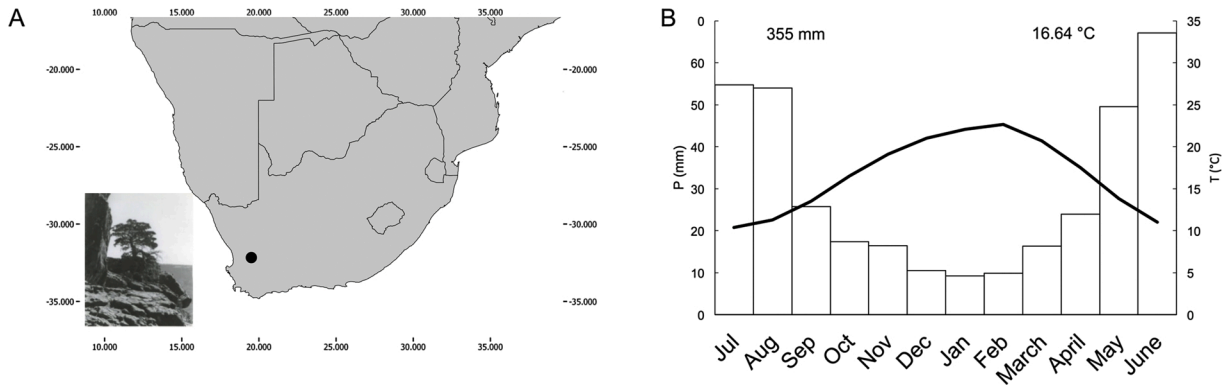

Fig. 1. (A) Study area with indication of the Die Bos site (indicated with dot) with a photograph of a *Widdringtonia cedarbergensis* tree (Valmore LaMarche Jr). (B) Average monthly temperature (bold line) and total monthly precipitation (bars) averaged over a wider region of the Die Bos Site in the cedarberg mountains (32.2-32.6 °S and 19.1.-19.3 °E) with mean annual precipitation sums (355 mm) and mean annual temperature (16.6 °C) for the period 1901 – 2018. The climate data were extracted from CRU TS4.03 0.5 ° gridded data set (Mitchell and Jones, 2005).

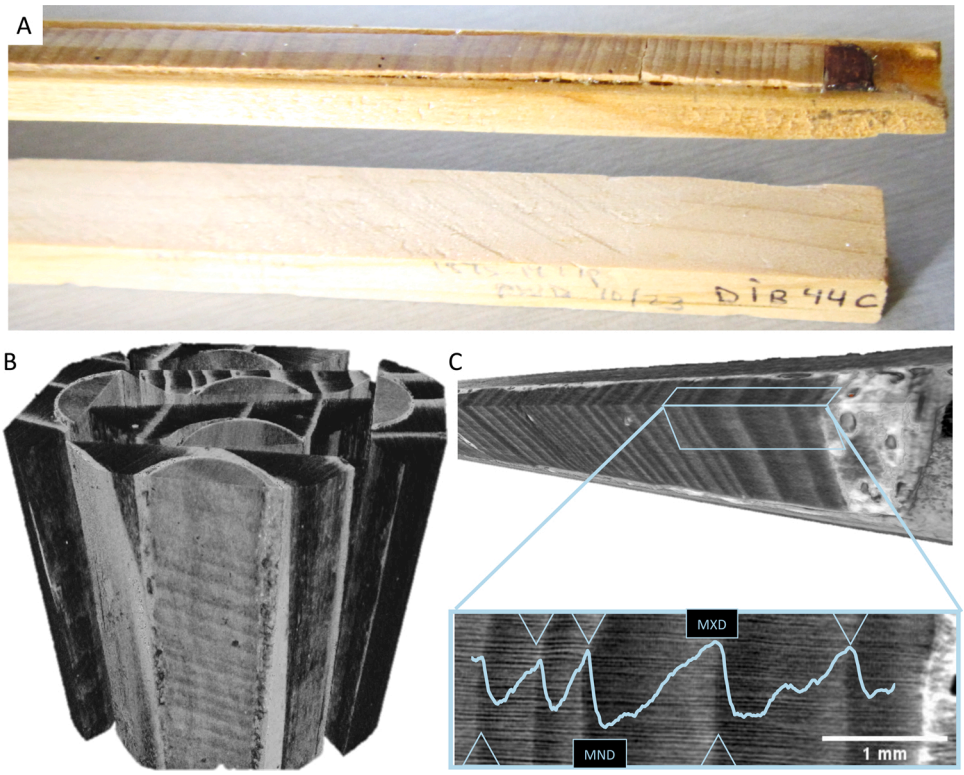

Fig. 2. (A) A *Widdringtonia cedarbergensis* sample from the Die Bos site (sampled in March 1978 and currently in the UA LTRR collection), where the mount was cut to fit into the X-ray CT foam sample holder (B) 3D rendering of an X-ray CT image stack, showing the sample holder with 6 cores (mount and glue still attached),. (C) Section of a sample, wherein a volume of core is selected that only contains WICE wood and no glue or mount (D) Transversal slice of an X-ray CT volume of WICE wood showing the ring boundaries (open triangles) and density variations in grey values. The corresponding density profile (in pale blue) with indication of minimum density (MND) and maximum density (MXD). Rendering was done in VGStudio Max (Volume Graphics). Resolution of the reconstructed volumes is 10 µm.

high-energy CT scanner optimized for research, developed by the UGent Centre for X-ray tomography (Masschaele et al., 2013), controlled by a LabVIEW® based software platform (Dierick et al., 2010). The acquired projections were reconstructed to 3D volumes using Octopus Reconstruction (Vlassenbroeck et al., 2007). Separate volumes were then stitched together using a custom-written macro routine in ImageJ, based on a stitching algorithm (Preibisch et al., 2009). Within the resulting digital volume of each sample holder that holds the cores (Fig. 2B), we labelled and cropped individual cores and further selected volumes to avoid having glue and support in the final 3D core with ImageJ (Fig. 2C) (Schneider et al., 2012). For some sections within the cores we were unable to measure density, as there was not enough core volume left due to excessive sanding (Fig. S2).

We further treated the 3D images using the Densitometry Toolbox software (De Mil et al., 2016), available on www.dendrochronomics.ugent.be. First, we loaded the 3D images into the graphical user interface, where we measured the rings on the transversal and radial plane. After both correcting for ring and grain angle (Van den Bulcke et al., 2014), a density profile is obtained from this 3D image. Subsequently, MND and MXD are calculated as the minimal and maximal value of that profile within a given year (Fig. 2C). After verifying our ring indications made in the software with the years marked on the cores (Dunwiddie and LaMarche, 1980) and the TRW data from the ITRDB, we exported TRW, MND, and MXD series for further analysis.

We measured MXBI at 1400 DPI (which equals ~ 18 µm resolution) using a flatbed scanner (EPSON 10,000 XL) using the Windendro 2014 software (Regents Instruments). We measured MXBI for the most recent portion of the crossdated cores (1901–1978) and removed the MXBI measurement of the most recent ring, which often had very little latewood (due to sampling seasonality and adjacency to the bark) and hence artificially low MXBI values (Rydval et al., 2014) (Figs. 2A, S1).

2.4. Isotope analysis

For stable isotope analyses of C and O, a subset of four trees with high TRW inter-series correlations were selected. Because the tree cores were mounted with a water-soluble glue, a simple immersion in hot water was sufficient to remove the glue and process the tree cores for cellulose extraction and stable isotope measurements. Annual growth rings were manually separated using a razor blade. The wood samples were ground to 20 meshes and α-cellulose was extracted following the protocol described in Leavitt (1993), including the addition of NaOH to remove hemicellulose. The α-cellulose extracted from each sample underwent a sonication step to ensure homogenization. $\delta^{13}C$ and $\delta^{18}O$ were measured for 30 years (1948-1978 CE) from each tree (n = 4). Subsamples of 0.15 and 0.30 mg of the resultant cellulose were measured for $\delta^{13}C$ and $\delta^{18}O$, respectively, using an isotope-ratio mass spectrometer at the University of Maryland (Evans et al., 2016). Isotopic values were compared to the $\delta^{13}C$ Vienna Peedee belemnite (VPD) ‰ and $\delta^{18}O$ Vienna Standard Mean Ocean Water (VSMOW) ‰ reference standards.

The overall precision of the isotope measurements based on replicate standard analyses was 0.11 and 0.31 for $\delta^{13}C$ and $\delta^{18}O$ respectively. The $\delta^{13}C$ time series were corrected for the atmospheric $\delta^{13}C$ decline following the procedure described in McCarroll et al. (2009) and using the compiled atmospheric $\delta^{13}C$ data from Belmecheri and Lavergne (2020). In addition to this data, a pooled $\delta^{13}C$ dataset from other Die Bos samples (February and Stock, 1999) was used to compare our series against.

2.5. Chronology development

We analyzed all series in R studio 1.2.1335 (Rstudio 2019) using the dplR library (Bunn, 2008).

We then calculated the Expressed Population Signal (EPS) and the total mean interseries correlation (RBAR). We removed the age trend from individual TRW series using a negative exponential curve and using a spline of 30 years for the density and MXBI series (Cook and Peters, 1981). We developed the TRW, MND, MXD, and MXBI chronologies by calculating bi-weight averages of the detrended individual series. We compared the chronologies of these parameters using a pairwise correlation matrix.

2.6. Climate data and climate-correlation analysis

The weather variables of interest are temperature and precipitation. In order to look at possible variations between weather stations, we compared the data with the CRU TS4.03 0.5 ° gridded data set (Mitchell and Jones, 2005). For precipitation, we compared the available weather station data being Clanwilliam (32.18 °S 18.90 °E), Algeria (32.37 °S 19.06 °E), Citrusdal (32.59 °S 19.01 °E), Langgewens (33.28 °S,18.70 °E) and Wupperthal 32.28 °S 19.22 °E) and these covary significantly with the CRU data (r = 0.70−0.96 (P < 0.001), Fig. S3 B, D).

For temperature, there are only a limited number of stations in the wider region, and those nearby only cover a short period that is not fully overlapping with our tree-ring series. Temperature data were available from Cape Town (33.90 °S 18.50 °E), Okiep (29.60 °S 17.88 °E), Langgewens (33.28 °S 18.70 °E) and Calvinia (31.47 ° S 19.77 °E).

These station temperature data covary significantly with the CRU TS4.03 0.5 ° gridded dataset (ranging from r = 0.58−0.94, P < 0.05, Fig. S3 C, E).

These sparse data often do not optimally represent climate variations at a regional scale. Therefore, monthly precipitation sums and temperature averages were extracted from the CRU TS4.03 0.5 ° gridded data set (Mitchell and Jones, 2005) for a region covering the Die Bos site (−32.2 – 32.6 °S, 19.1 – 19.3 °E) for the 1930−1978 period, for which reliable temperature and precipitation data and tree-ring data overlap.

We performed correlation analyses between the various tree-ring parameters (TRW, MXD, MND, MXBI, $\delta^{13}C$, and $\delta^{18}O$) and monthly and seasonal 3-month intervals (Meko et al., 2011) of precipitation and temperature data using the TreeClim package (Zang and Biondi, 2014). We expanded the dendroclimatic analysis from previous-season May to current-season June, to consider the full potential growing season of WICE.

Additionally, we developed field correlation maps for each grid cell in the region using the KNMI Climate Explorer (Trouet and Van Oldenborgh, 2013). Data and analysis scripts of the presented results are available through Mendeley Data https://doi.org/10.17632/gctzb4z348.1.

3. Results

3.1. Tree-ring width and density chronologies

RBAR values were higher for TRW than for MND and MXD (Table 1). RBAR- and EPS-values were high for MXBI, despite the low number of samples. The MND and TRW chronologies were significantly negatively correlated with each other (r=-0.35; p < 0.01), whereas MXD and MXBI were significantly positively correlated (r = 0.67; p < 0.01) (Fig. 3; Table 2). The $\delta^{18}O$ and $\delta^{13}C$ series were significantly positively correlated with each other (r = 0.69; p < 0.01) (Fig. 4; Table 2) and with the MXD series (r = 0.43, 0.48, resp.), but not with MXBI (Table 2). RBAR was acceptable and EPS-values exceeded the 0.85 threshold for the $\delta^{18}O$ series, but not for the $\delta^{13}C$ series.

3.2. Dendroclimatic analysis

We found that cell lumina were largest, and thus density was at a minimum, in the earlywood of WICE (Fig. S4). MND correlates significantly negatively with previous-year autumn (June) and negative current-year spring (October to November) precipitation, but not with temperature (Fig. 5A, B).

TRW, on the other hand, is positively correlated with current-year November precipitation (Fig. 5C, D) and negatively with November to December temperature (Fig. 5C). MXD is significantly negatively correlated with current summer (January-March) precipitation (Fig. 5E), as well as current May temperature. This temperature correlation covers a large zone in southwestern Africa (Fig. 5F). MXBI has no significant temperature correlations, but is influenced by current January-May precipitation (Fig. S5).

The $\delta^{18}O$ chronology (the average of 4 individual-tree $\delta^{18}O$ series) was generally positively correlated with temperature and negatively with precipitation, but correlations were weak, apart from a negative September and December influence of temperature and a positive September response to precipitation (Fig. S7). Due to low RBAR statistics (Table 1), the $\delta^{13}C$ chronology was not considered in further analysis. Adding previous pooled measurements from $\delta^{13}C$ on trees of the Die Bos site (February and Stock, 1999) only yielded a small increase in RBAR and EPS (0.28 versus 19 and 0.66 versus 0.49 respectively) (Fig. S8) and no conclusive dendroclimatic signal as well (data not shown). Spatial correlations for $\delta^{18}O$ and $\delta^{13}C$ with monthly precipitation and temperature were insignificant (data not shown).

Table 1
Sample size (N) and mean interseries correlation (RBAR) and Expressed Population Signal (EPS) for tree ring width (TRW), maximum latewood density (MXD), minimum density (MND), maximum latewood blue intensity (MXBI), and stable isotopes ($\delta^{18}O$ and $\delta^{13}C$).

Tree-ring parameter	N cores (trees)	Period	RBAR	EPS
TRW	20 (10)	1930−1978	0.393	0.891
MXD	20 (10)	1930−1978	0.174	0.736
MND	20 (10)	1930−1978	0.268	0.809
MXBI	10 (7)	1930−1977	0.627	0.949
$\delta^{18}O$	4 (4)	1948−1978	0.627	0.87
$\delta^{13}C$	4 (4)	1948−1978	0.19	0.484

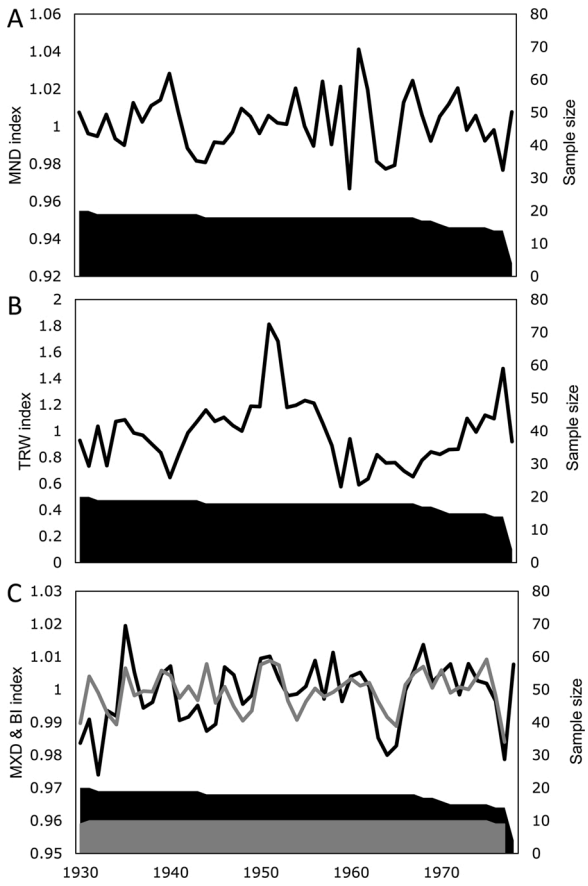

Fig. 3. (A) Minimum Density (MND) (B) Tree-Ring Width (TRW) (C) Maximum Latewood Density (MXD) (black), and Blue Intensity (BI) (grey) chronologies (1930-1978) of *Widdringtonia cedarbergensis* from the Die Bos dataset. Shaded area marks the sample depth.

Table 2
Pearson correlation values between the Minimum Density (MND), Tree-Ring Width (TRW), Maximum Latewood Density (MXD), and Maximum Latewood Blue Intensity (MXBI) chronologies of *Widdringtonia cedarbergensis* from the Die Bos dataset. Significant correlations are marked with * ($P < 0.05$) and ** ($P < 0.01$).

	MND	TRW	MXD	MXBI	$\delta^{18}O$
TRW	−0.35**				
MXD	0.32**	−0.11			
MXBI	0.10	−0.10	0.67**		
$\delta^{18}O$	0.27	0.43*	0.43*	0.33	
$\delta^{13}C$	0.34	0.20	0.48**	0.34	0.69**

4. Discussion

The inverse relation between MND and October-November precipitation (Fig. 5A, B) suggests that spring moisture availability stimulates the formation of large cell lumina (Camarero et al., 2014) and thus a lower wood density (Rathgeber, 2017). Spring precipitation response has also been reported in MND series of other conifer species from Mediterranean regions (Camarero and Hevia, 2020) and is thus expected here in the Mediterranean climate of the winter rainfall zone in South Africa, given the similarity of precipitation seasonality and average growing season temperature. The secondary response to previous seasonal winter (June-August) precipitation (Fig. 5A) is often influenced by climate conditions prior to the actual growing season that influence carbon storage and availability at the start of the growing season (e.g. Szejner et al., 2018).

The relationship between TRW and spring precipitation, on the other hand, is positive with more October-November precipitation resulting in wider rings (Fig. 5C, D). The inverse dendroclimatic signal in MND vs. TRW can thus be explained by the inverse relation between these tree-ring parameters (Table 2, Fig. 3A, B) and by the association between large lumina, resulting in low density, and wide rings (Hughes et al., 1994).

We found that the spring precipitation signal is stronger for MND (r-values up to 0.51 for October-November-December) than for TRW (r-values up to 0.41 for October-November-December), which is possibly related to the generally observed lower autocorrelation values in density series compared to TRW (Schneider et al., 2015) as shown in Fig. S6. On the other hand, the positive spring precipitation signal in TRW was complemented by a negative influence of spring temperature (Fig. 5C), which reflects a negative tree-growth response to high spring temperatures and associated lack of precipitation. The dendroclimatic potential of WICE TRW has previously been shown by Dunwiddie and LaMarche (1980), who reported spring precipitation and temperature responses that were of the same sign but weaker (r-values up to ~0.2) than the responses in our study. This weaker climatic signal can be explained by a combination of a shorter correlation period, as well as temperature and precipitation data from different weather stations (data not accessible to us).

MXD and MXBI are both estimates of cell wall thickness and lumen area in the latewood (Björklund et al., 2019; Reid and Wilson, 2020) and they are significantly positively correlated with each other in WICE (Table 2, Fig. 3C). The climatic signal of precipitation was similar (Figs. S5, 5 E; (Kaczka et al., 2018)), but was generally weaker for temperature in MXBI compared to MXD, which is in line with the results found in Reid and Wilson (2020). Possibly the resin ducts and the surfacing had an effect on the MXBI measurements whereas X-ray CT does not require surface treatment. In contrast to other MXD studies at high-elevation Mediterranean sites (Büntgen et al., 2010; Klesse et al., 2015; Trouet et al., 2012), we found only weak negative correlations between MXD and May temperature (Figs. 5E, S1). Negative fall temperature influence on MXD has also been recorded in other SH tree

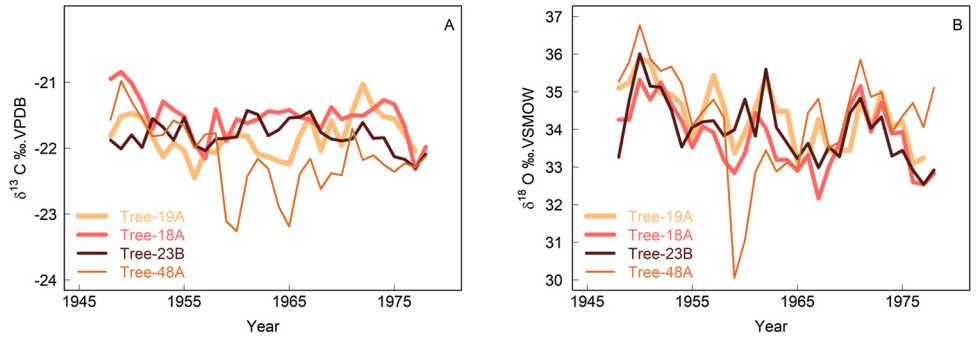

Fig. 4. Individual tree (n = 4) time series of $\delta^{13}C$ (A) and $\delta^{18}O$ (B) series of *Widdringtonia cedarbergensis* samples from the Die Bos collection.

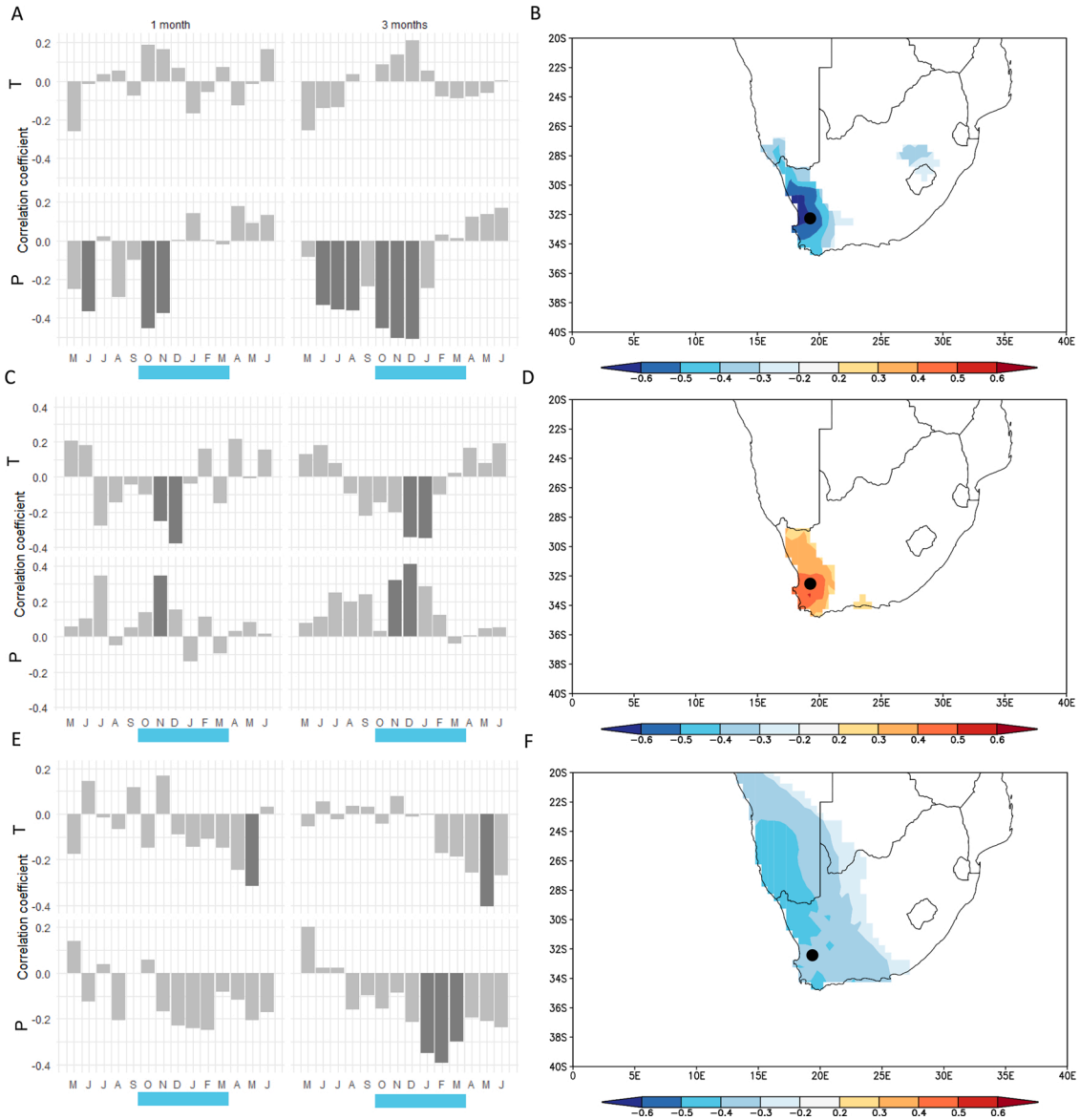

Fig. 5. Pearson correlation coefficients (1930-1978) between monthly temperature (T) and precipitation (P) values (CRU TS4.03 for -32.4 ° S, 19.22) and (A) MND, (C) TRW, and (E) MXD chronologies. Spatial correlation maps ($P < 0.1$) between (B) MND and October-November precipitation, (D) TRW and November-December precipitation, and (F) MXD and April-May temperature (CRU TS.4.03). Significant correlations ($P < 0.05$) are marked in dark grey. Maps were generated using the KNMI explorer (Trouet and Van Oldenborgh, 2013). Sampling location is marked by dot and growing season is indicated with blue bar below the respective months. (For interpretation of the references to colour in the Figure, the reader is referred to the web version of this article).

species, for instance in Huon pine in Tasmania (Drew et al., 2013) and manoao (silver pine) in New Zealand (Blake et al., 2020) and was explained by higher fall temperatures reducing the duration of secondary cell wall thickening phase (which results in lower MXD values). Nevertheless, the temperature signal in MXD is weak in our study (Fig. 5E, F) and, like other low-latitude MXD temperature signals, likely insufficient for climate reconstruction (Esper et al., 2006), but could possibly be improved upon with higher sample replication (Cao et al., 2020). Along with the negative relation with temperature, we found a negative influence of summer (January-March) precipitation on MXD, which could be due to favorable conditions for growth and associated wider lumina in the latewood. Similar influence can be found for the MXBI, but more pronounced and later in the season (January-May) (Fig. S5). A potentially prolonged growing season (see Fig. 5 A,C,E) could explain both the May temperature and January-March precipitation influence on MXD as well as the January-May precipitation influence on MXBI. In addition to this, findings based on the growing season (February et al., 2007), unclear tree-ring boundaries and intra-annual bands (February and Stock, 1998) and observations from Fig. S1 confirm that there could be resumption of growth after March due to favourable conditions. Given the limited annual woody increment of WICE trees from this study (+-1.001 mm in the given 1930–1978 period) and a previous study (February et al., 2007), the winter rainfall could also have caused a swelling of the bark in June-August, more than the actual woody growth (e.g., (Zweifel and Häsler, 2001)). Additional ecophysiological studies, particularly using cambial xylogenesis and phenology techniques, might be necessary to precisely determine the cambial growing season.

Time series of all tree-ring parameters, apart from $\delta^{13}C$, show strong common variance amongst individual samples, as reflected by acceptable RBAR and EPS-values (Table 1), given the limited number of samples. The limited common variance of the $\delta^{13}C$ time series (Fig. 4A, Table 1, Fig. S8) can be explained by the low sample size (n = 4), but can as well as be related to micro-climate and soil moisture (slope) status of

the individual trees, which would translate into different stress status and thus $\delta^{13}C$ values. Nevertheless, the combined WICE $\delta^{13}C$ series showed similar interannual variability to the $\delta^{18}O$ series (Fig. 4, Table 2). Despite high RBAR, we found no relevant significant climate responses for $\delta^{18}O$ (Fig. S7). The lack of significant climate response of tree-ring $\delta^{18}O$ possibly stems from complex interplay between variations in source water $\delta^{18}O$ (precipitation, soil water) and relative humidity effects on stomatal conductance and therefore evaporative enrichment at the leaf level (Roden and Ehleringer, 1999). However, further investigation using proxy forward modelling could be useful in order to assess the tree-ring $\delta^{18}O$ sensitivity to variations in relative humidity (vs source water) (Belmecheri et al., 2018). A study on the $\delta^{18}O$ composition of xylem water from WICE show similar patterns of xylem water and precipitation $\delta^{18}O$ series that reflect a rainout source water from the nearby Atlantic ocean; small interannual variations indicate a constant source except for rain events related to cyclone activities originating from the East (February et al., 2007). This suggests that potential variation in tree-ring $\delta^{18}O$ would be driven by variations in evaporative enrichment in response to soil moisture and relative humidity status.

Most WICE tree-ring parameters (MND, TRW, MXD, MXBI) are thus sensitive to precipitation in the spring, summer months (October to March), when the majority of woody tree growth is hypothesized to occur (Dunwiddie and LaMarche, 1980). The Die Bos site is located at mid-elevation and mid-latitude, where precipitation primarily falls as rain rather than as snow. In contrast to higher-elevation Mediterranean sites, such as the Sierra Nevada in California, or the Pyrenees and mountain ranges in the Balkans in southern Europe, winter precipitation at Die Bos is thus less stored in snow on the landscape and less available when the trees start growing in spring. This can explain why, unlike other high-elevation Mediterranean tree-ring chronologies (Büntgen et al., 2010; Klesse et al., 2015; Szymczak et al., 2020), our WICE chronologies are sensitive to spring and summer, rather than winter precipitation.

The climatic signal in individual tree-ring parameters is relatively weak (up to r=-0.51 for October-December precipitation in MND), but could be improved by increasing sample replication and expanding the calibration period to more than the 30–47 years investigated here. Moreover, the seasonal confluence of responses across multiple parameters suggests potential for multi-parameter climate reconstruction, particularly of spring precipitation. Such multi-parameter climate reconstructions have, for instance, been successfully developed for the Bighorn Mountains in the Western USA (Hudson et al., 2019). Our study focused on the twentieth century portion of an existing WICE sample collection, which extends back to the 16th century and could thus be used as a base for a 350+-year long, annually resolved precipitation reconstruction unique to southern Africa. To optimize such a climate reconstruction, the Dunwiddie and LaMarche (1980) sample set, which was collected in 1978, will have to be updated to the present to capture recent climatic changes and trends. The Mediterranean region of South Africa is particularly vulnerable to climate change and a precipitation reconstruction could contribute to placing current and projected anthropogenic change in the context of past natural climate variability.

Declaration of Competing Interest

All authors have no conflict of interests to declare.

Acknowledgments

Tom De Mil received a Léon Speeckaert Fund postdoctoral fellowship from the King Baudouin Foundation and the Belgian American Educational Foundation (BAEF). Matt Meko and Valerie Trouet were supported by a National Science Foundation CAREER grant (AGS-1349942) and by a grant from the College of Science at the University of Arizona. The Special Research Fund of Ghent University is acknowledged for the support to the UGCT Centre of Expertise (BOF.EXP.2017.0007). Thanks to Katie Marascio for isotope sample processing. Thanks to Hans Beeckman (Royal Museum for Central Africa) for providing wood anatomical information and microsections from the xylarium collection. Thanks to Stijn Willen (UGent-Woodlab, Ghent University) for sample preparation and to Ivan Josipovic (UGCT, Ghent University), who optimized the X-ray CT scanning process and 3D rendering. Thanks to Peter Brewer, Rika du Plessis, Jasper Slingsby, David Le Maitre, Louise Esterhuizen and Carl Pretorius for providing and checking information on the growing season of *Widdringtonia cedarbergensis*. Grateful to Amy Hudson, Guobao Xu, Diana Zamora-Reyes from the Trouet Lab and other colleagues, staff and faculty from the Laboratory of Tree-Ring Research, University of Arizona.

Appendix A. Supplementary data

Supplementary material related to this article can be found, in the online version, at doi:https://doi.org/10.1016/j.dendro.2021.125879.

References

Ahmed, M., Anchukaitis, K.J., Asrat, A., Borgaonkar, H.P., Braida, M., Buckley, B.M., Büntgen, U., Chase, B.M., Christie, D.A., Cook, E.R., Curran, M.A.J., Diaz, H.F., Esper, J., Fan, Z.X., Gaire, N.P., Ge, Q., Gergis, J., González-Rouco, J.F., Goosse, H., Grab, S.W., Graham, N., Graham, R., Grosjean, M., Hanhijärvi, S.T., Kaufman, D.S., Kiefer, T., Kimura, K., Korhola, A.A., Krusic, P.J., Lara, A., Lézine, A.M., Ljungqvist, F.C., Lorrey, A.M., Luterbacher, J., Masson-Delmotte, V., McCarroll, D., McConnell, J.R., McKay, N.P., Morales, M.S., Moy, A.D., Mulvaney, R., Mundo, I.A., Nakatsuka, T., Nash, D.J., Neukom, R., Nicholson, S.E., Oerter, H., Palmer, J.G., Phipps, S.J., Prieto, M.R., Rivera, A., Sano, M., Severi, M., Shanahan, T.M., Shao, X., Shi, F., Sigl, M., Smerdon, J.E., Solomina, O.N., Steig, E.J., Stenni, B., Thamban, M., Trouet, V., Turney, C.S.M., Umer, M., van Ommen, T., Verschuren, D., Viau, A.E., Villalba, R., Vinther, B.M., Von Gunten, L., Wagner, S., Wahl, E.R., Wanner, H., Werner, J.P., White, J.W.C., Yasue, K., Zorita, E., 2013. Continental-scale temperature variability during the past two millennia. Nat. Geosci. 6, 339–346. https://doi.org/10.1038/ngeo1797.

Allen, K., Drew, D.M., Downes, G.M., Evans, R., Baker, P., Grose, M., 2012. Ring width, climate and wood density relationships in two long-lived Tasmanian tree species. Dendrochronologia 30, 167–177. https://doi.org/10.1016/j.dendro.2010.12.006.

Allen, K.J., Cook, E.R., Evans, R., Francey, R., Buckley, B.M., Palmer, J.G., Peterson, M.J., Baker, P.J., 2018. Lack of cool, not warm, extremes distinguishes late 20th Century climate in 979-year Tasmanian summer temperature reconstruction. Environ. Res. Lett. 13 https://doi.org/10.1088/1748-9326/aaafd7.

Allen, K.J., Anchukaitis, K.J., Grose, M.G., Lee, G., Cook, E.R., Risbey, J.S., O'Kane, T.J., Monselesan, D., O'Grady, A., Larsen, S., Baker, P.J., 2019. Tree-ring reconstructions of cool season temperature for far southeastern Australia, 1731–2007. Clim. Dyn. 53, 569–583. https://doi.org/10.1007/s00382-018-04602-2.

Anchukaitis, K.J., Wilson, R., Briffa, K.R., Büntgen, U., Cook, E.R., D'Arrigo, R., Davi, N., Esper, J., Frank, D., Gunnarson, B.E., Hegerl, G., Helama, S., Klesse, S., Krusic, P.J., Linderholm, H.W., Myglan, V., Osborn, T.J., Zhang, P., Rydval, M., Schneider, L., Schurer, A., Wiles, G., Zorita, E., 2017. Last millennium Northern Hemisphere summer temperatures from tree rings: part II, spatially resolved reconstructions. Quat. Sci. Rev. 163, 1–22. https://doi.org/10.1016/j.quascirev.2017.02.020.

Andreu-Hayles, L., Ummenhofer, C.C., Barriendos, M., Schleser, G.H., Helle, G., Leuenberger, M., Gutiérrez, E., Cook, E.R., 2017. 400 Years of summer hydroclimate from stable isotopes in Iberian trees. Clim. Dyn. https://doi.org/10.1007/s00382-016-3332-z.

Archer, E., Landman, W., Malherbe, J., Tadross, M., Pretorius, S., 2019. South Africa's winter rainfall region drought: a region in transition? Clim. Risk Manag. 25, 100188 https://doi.org/10.1016/j.crm.2019.100188.

Belmecheri, S., Lavergne, A., 2020. Compiled records of atmospheric CO2 concentrations and stable carbon isotopes to reconstruct climate and derive plant ecophysiological indices from tree rings. Dendrochronologia 63, 125748. https://doi.org/10.1016/j.dendro.2020.125748.

Belmecheri, S., Wright, W.E., Szejner, P., Morino, K.A., Monson, R.K., 2018. Carbon and oxygen isotope fractionations in tree rings reveal interactions between cambial phenology and seasonal climate. Plant Cell Environ. 41, 2758–2772. https://doi.org/10.1111/pce.13401.

Björklund, Ja., Gunnarson, B.E., Seftigen, K., Esper, J., Linderholm, H.W., 2014. Blue intensity and density from northern Fennoscandian tree rings, exploring the potential to improve summer temperature reconstructions with earlywood information. Clim. Past Discuss. 10, 877–885. https://doi.org/10.5194/cp-10-877-2014.

Björklund, J., Seftigen, K., Schweingruber, F., Fonti, P., von Arx, G., Bryukhanova, M.V., Cuny, H.E., Carrer, M., Castagneri, D., Frank, D.C., 2017. Cell size and wall dimensions drive distinct variability of earlywood and latewood density in Northern Hemisphere conifers. New Phytol. https://doi.org/10.1111/nph.14639.

Björklund, J., Arx, G., Nievergelt, D., Wilson, R., Van den Bulcke, J., Günther, B., Loader, N.J., Rydval, M., Fonti, P., Scharnweber, T., Andreu-Hayles, L., Büntgen, U., D'Arrigo, R., Davi, N., De Mil, T., Esper, J., Gärtner, H., Geary, J., Gunnarson, B.E., Hartl, C., Hevia, A., Song, H., Janecka, K., Kaczka, R.J., Kirdyanov, A.V.,

Kochbeck, M., Liu, Y., Meko, M., Mundo, I., Nicolussi, K., Oelkers, R., Pichler, T., Sánchez-Salguero, R., Schneider, L., Schweingruber, F., Timonen, M., Trouet, V., Van Acker, J., Verstege, A., Villalba, R., Wilmking, M., Frank, D., 2019. Scientific merits and analytical challenges of tree-ring densitometry. Rev. Geophys. https://doi.org/10.1029/2019rg000642.

Blake, S.A.P., Palmer, J.G., Björklund, J., Harper, J.B., Turney, C.S.M., 2020. Palaeoclimate potential of New Zealand Manoao colensoi (silver pine) tree rings using Blue-Intensity (BI). Dendrochronologia 60, 125664. https://doi.org/10.1016/j.dendro.2020.125664.

Bunn, A.G., 2008. A dendrochronology program library in R (dplR). Dendrochronologia 26, 115–124. https://doi.org/10.1016/j.dendro.2008.01.002.

Büntgen, U., Frank, D., Trouet, V., Esper, J., 2010. Diverse climate sensitivity of Mediterranean tree-ring width and density. Trees - Struct. Funct. 24, 261–273. https://doi.org/10.1007/s00468-009-0396-y.

Büntgen, U., Tegel, W., Nicolussi, K., McCormick, M., Frank, D., Trouet, V., Kaplan, J., Herzig, F., Heussner, K., Wanner, H., Luterbacher, J., Esper, 2011. 2500 years of european climate variability and human susceptibility. Science (80-) 331, 578–582.

Camarero, J.J., Hevia, A., 2020. Links between climate, drought and minimum wood density in conifers. IAWA J. 0, 1–20. https://doi.org/10.1163/22941932-bja10005.

Camarero, J.J., Rozas, V., Olano, J.M., 2014. Minimum wood density of Juniperus thurifera is a robust proxy of spring water availability in a continental Mediterranean climate. J. Biogeogr. 41, 1105–1114. https://doi.org/10.1111/jbi.12271.

Camarero, J.J., Fernández-Pérez, L., Kirdyanov, A.V., Shestakova, T.A., Knorre, A.A., Kukarskih, V.V., Voltas, J., 2017. Minimum wood density of conifers portrays changes in early season precipitation at dry and cold Eurasian regions. Trees - Struct. Funct. 31, 1423–1437. https://doi.org/10.1007/s00468-017-1559-x.

Campbell, R., Grudd, H., Robertson, I., Loader, N.J., Gunnarson, B., McCarroll, D., 2011. Blue Intensity in Pinus sylvestris Tree Rings: A Manual for A New Palaeoclimate Proxy. Tree-Ring Res. 67, 127–134. https://doi.org/10.3959/2010-13.1.

Cao, X., Fang, K., Chen, P., Zhang, P., Björklund, J., Pumijumnong, N., Guo, Z., 2020. Microdensitometric records from humid subtropical China show distinct climate signals in earlywood and latewood. Dendrochronologia 64. https://doi.org/10.1016/j.dendro.2020.125764.

Chase, B.M., Meadows, M.E., 2007. Late Quaternary dynamics of southern Africa's winter rainfall zone. Earth-Science Rev. 84, 103–138. https://doi.org/10.1016/j.earscirev.2007.06.002.

Chase, B.M., Lim, S., Chevalier, M., Boom, A., Carr, A.S., Meadows, M.E., Reimer, P.J., 2015. Influence of tropical easterlies in southern Africa's winter rainfall zone during the Holocene. Quat. Sci. Rev. 107, 138–148. https://doi.org/10.1016/j.quascirev.2014.10.011.

Colombaroli, D., Cherubini, P., De Ridder, M., Saurer, M., Toirambe, B., Zweifel, N., Beeckman, H., 2016. Stable carbon and oxygen isotopes in tree rings show physiological responses of Pericopsis elata to precipitation in the Congo Basin. J. Trop. Ecol. 1–13. https://doi.org/10.1017/S0266467416000134.

Cook, E., Peters, K., 1981. The smoothing spline, a new approach to standardising forest interior tree-ring. Trre-ring Bull. 41, 45–53.

De Mil, T., Vannoppen, A., Beeckman, H., Van Acker, J., Van den Bulcke, J., 2016. A field-to-desktop toolchain for X-ray CT densitometry enables tree ring analysis. Ann. Bot. 117, 1187–1196. https://doi.org/10.1093/aob/mcw063.

De Mil, T., Hubau, W., Angoboy Ilondea, B., Rocha Vargas, M.A., Boeckx, P., Steppe, K., Van Acker, J., Beeckman, H., Van den Bulcke, J., 2019. Asynchronous leaf and cambial phenology in a tree species of the Congo Basin requires space–time conversion of wood traits. Ann. Bot. 245–253. https://doi.org/10.1093/aob/mcz069.

Dierick, M., Van Loo, D., Masschaele, B., Boone, M., Van Hoorebeke, L., 2010. A LabVIEW® based generic CT scanner control software platform. J. Xray Sci. Technol. 18, 451–461. https://doi.org/10.3233/XST-2010-0268.

Drew, D.M., Allen, K., Downes, G.M., Evans, R., Battaglia, M., Baker, P., 2013. Wood properties in a long-lived conifer reveal strong climate signals where ring-width series do not. Tree Physiol. 33, 37–47. https://doi.org/10.1093/treephys/tps111.

Dunwiddie, P.W., LaMarche, V.C., 1980. A climatically responsive tree-ring record from Widdringtonia cedarbergensis, Cape Province, South Africa. Nature 286, 796–797. https://doi.org/10.1038/286796a0.

Endfield, G.H., Nash, D.J., 2002. Missionaries and morals: climatic discourse in nineteenth-century central Southern Africa. Ann. Assoc. Am. Geogr. 92, 727–742. https://doi.org/10.1111/1467-8306.00313.

Esper, J., Buntgen, U., Frank, D., Nievergelt, D., Verstege, A., 2006. Multi tree-ring parameters from Atlas cedar (Morocco) and their climatic signal. Tree Rings Archaeol. Climatol. Ecol. 4, 46–55.

Evans, M.N., Selmer, K., Breeden, I., Lopatka, A., Plummer, R., 2016. Correction algorithm for online continuous flow D13C and D18O carbonate and cellulose stable isotope analysis. Geochem. Geophys. Geosyst. 17, 3580–3588. https://doi.org/10.1002/2015GC006205.Received.

February, E.C., Gagen, M., 2003. A dendrochronological assessment of two South African Widdringtonia species. S. Afr. J. Bot. 69, 428–433. https://doi.org/10.1016/S0254-6299(15)30326-4.

February, E.C., Stock, W.D., 1998. The relationship between ring width measures and precipitation for Widdringtonia cedarbergensis. S. Afr. J. Bot. 64, 213–216. https://doi.org/10.1016/S0254-6299(15)30870-X.

February, E.C., Stock, W.D., 1999. Declining trend in the 13C/12C ratio of atmospheric carbon dioxide from tree rings of South African Widdringtonia cedarbergensis. Quat. Res. 52, 229–236. https://doi.org/10.1006/qres.1999.2057.

February, E.C., West, A.G., Newton, R.J., 2007. The relationship between rainfall, water source and growth for an endangered tree. Austral Ecol. 32, 397–402. https://doi.org/10.1111/j.1442-9993.2007.01711.x.

Fichtler, E., Worbes, M., 2012. Wood anatomical variables in tropical trees and their relation to site conditions and individual tree morphology. IAWA J. 33, 119–140. https://doi.org/10.1163/22941932-90000084.

Hannaford, M.J., Jones, J.M., Bigg, G.R., 2015. Early-nineteenth-century southern African precipitation reconstructions from ships' logbooks. Holocene 25, 379–390. https://doi.org/10.1177/0959683614557573.

Hudson, A.R., Alfaro-Sanchez, R., Babst, F., Belmecheri, S., Moore, D.J.P., Trouet, V., 2019. Seasonal and synoptic climatic drivers of tree growth in the Bighorn Mountains, WY, USA (1654–1983 CE). Dendrochronologia 58, 125633. https://doi.org/10.1016/j.dendro.2019.125633.

Hughes, M.K., Xiangding, W., Xuemei, S., Garfin, G.M., 1994. A preliminary reconstruction of rainfall in North-Central China since A.D. 1600 from Tree-Ring Density and Width. Quat. Res. 42, 88–99.

Jones, P.D., Briffa, K.R., Osborn, T.J., Lough, J.M., Van Ommen, T.D., Vinther, B.M., Luterbacher, J., Wahl, E.R., Zwiers, F.W., Mann, M.E., Schmidt, G.A., Ammann, C. M., Buckley, B.M., Cobb, K.M., Esper, J., Goosse, H., Graham, N., Jansen, E., Kiefer, T., Kull, C., Küttel, M., Mosley-Thompson, E., Overpeck, J.T., Riedwyl, N., Schulz, M., Tudhope, A.W., Villalba, R., Wanner, H., Wolff, E., Xoplaki, E., 2009. High-resolution palaeoclimatology of the last millennium: a review of current status and future prospects. Holocene 19, 3–49. https://doi.org/10.1177/0959683608098952.

Kaczka, R.J., Spyt, B., Janecka, K., Beil, I., Büntgen, U., Scharnweber, T., Nievergelt, D., Wilmking, M., 2018. Different maximum latewood density and blue intensity measurements techniques reveal similar results. Dendrochronologia 49, 94–101. https://doi.org/10.1016/j.dendro.2018.03.005.

Kaufman, D., McKay, N., Routson, C., Erb, M., Davis, B., Heiri, O., Zhilich, S., 2020. A global database of Holocene paleo-temperature records. Sci. Data 1–34. https://doi.org/10.1038/s41597-020-0445-3 (submitted.

Klesse, S., Ziehmer, M., Rousakis, G., Trouet, V., Frank, D., 2015. Synoptic drivers of 400 years of summer temperature and precipitation variability on Mt. Olympus, Greece. Clim. Dyn. 45, 807–824. https://doi.org/10.1007/s00382-014-2313-3.

Klippel, L., Krusic, P.J., Konter, O., St. George, S., Trouet, V., Esper, J., 2019. A 1200+ year reconstruction of temperature extremes for the northeastern Mediterranean region. Int. J. Climatol. 39, 2336–2350. https://doi.org/10.1002/joc.5955.

Lavergne, A., Daux, V., Villalba, R., Pierre, M., Stievenard, M., Srur, A.M., 2017. Improvement of isotope-based climate reconstructions in Patagonia through a better understanding of climate influences on isotopic fractionation in tree rings. Earth Planet. Sci. Lett. 459, 372–380. https://doi.org/10.1016/j.epsl.2016.11.045.

Leavitt, S.W., 1993. Environmental information from 13 C/ 12 C ratios of Wood. Geophysical Monograph, pp. 325–331. https://doi.org/10.1029/gm078p0325, 78.

Masschaele, B., Dierick, M., Loo, D.Van, Boone, M.N., Brabant, L., Pauwels, E., Cnudde, V., Hoorebeke, L.Van, 2013. HECTOR: a 240kV micro-CT setup optimized for research. J. Phys. Conf. Ser. 463 https://doi.org/10.1088/1742-6596/463/1/012012.

McCarroll, D., Loader, N.J., 2004. Stable isotopes in tree rings. Quat. Sci. Rev. 23, 771–801. https://doi.org/10.1016/j.quascirev.2003.06.017.

McCarroll, D., Gagen, M.H., Loader, N.J., Robertson, I., Anchukaitis, K.J., Los, S., Young, G.H.F., Jalkanen, R., Kirchhefer, A., Waterhouse, J.S., 2009. Correction of tree ring stable carbon isotope chronologies for changes in the carbon dioxide content of the atmosphere. Geochim. Cosmochim. Acta 73, 1539–1547. https://doi.org/10.1016/j.gca.2008.11.041.

Meko, D.M., Touchan, R., Anchukaitis, K.J., 2011. Seascorr: a MATLAB program for identifying the seasonal climate signal in an annual tree-ring time series. Comput. Geosci. 37, 1234–1241. https://doi.org/10.1016/j.cageo.2011.01.013.

Mitchell, T.D., Jones, P.D., 2005. An improved method of constructing a database of monthly climate observations and associated high-resolution grids. Int. J. Climatol. 25, 693–712. https://doi.org/10.1002/joc.1181.

Morino, K., Minor, R.L., Barron-Gafford, G.A., Brown, P.M., Hughes, M.K., 2021. Bimodal cambial activity and false-ring formation in conifers under a monsoon climate. Tree Physiol. 1–13. https://doi.org/10.1093/treephys/tpab045.

Mundo, I.A., El Mujtar, V.A., Perdomo, M.H., Gallo, L.A., Villalba, R., Barrera, M.D., 2010. Austrocedrus chilensis growth decline in relation to drought events in northern Patagonia. Argentina. Trees - Struct. Funct. 24, 561–570. https://doi.org/10.1007/s00468-010-0427-8.

Neukom, R., Nash, D.J., Endfield, G.H., Grab, S.W., Grove, C.A., Kelso, C., Vogel, C.H., Zinke, J., 2014. Multi-proxy summer and winter precipitation reconstruction for southern Africa over the last 200 years. Clim. Dyn. 42, 2713–2726. https://doi.org/10.1007/s00382-013-1886-6.

Ngoma, J., Speer, J.H., Vinya, R., Kruijt, B., Moors, E., Leemans, R., 2017. The dendrochronological potential of Baikiaea plurijuga in Zambia. Dendrochronologia 41, 65–77. https://doi.org/10.1016/j.dendro.2016.05.002.

Nicholson, S.E., Klotter, D., Dezfuli, A.K., 2012. Spatial reconstruction of semi-quantitative precipitation fields over Africa during the nineteenth century from documentary evidence and gauge data. Quat. Res. (United States) 78, 13–23. https://doi.org/10.1016/j.yqres.2012.03.

O'Donnell, A.J., Allen, K.J., Evans, R.M., Cook, E.R., Trouet, V., Baker, P.J., 2016. Wood density provides new opportunities for reconstructing past temperature variability from southeastern Australian trees. Glob. Planet. Change 141, 1–11. https://doi.org/10.1016/j.gloplacha.2016.03.010.

Olano, J.M., Arzac, A., García-Cervigón, A.I., von Arx, G., Rozas, V., 2013. New star on the stage: amount of ray parenchyma in tree rings shows a link to climate. New Phytol. 198, 486–495. https://doi.org/10.1111/nph.12113.

Polgar, C.A., Primack, R.B., 2011. Leaf-out phenology of temperate woody plants: from trees to ecosystems. New Phytol. 191, 926–941. https://doi.org/10.1111/j.1469-8137.2011.03803.x.

Preibisch, S., Saalfeld, S., Tomancak, P., 2009. Globally optimal stitching of tiled 3D microscopic image acquisitions. Bioinformatics 25, 1463–1465. https://doi.org/10.1093/bioinformatics/btp184.

Pritzkow, C., Wazny, T., Heußner, K.U., Słowiński, M., Bieber, A., Liñán, I.D., Helle, G., Heinrich, I., 2016. Minimum winter temperature reconstruction from average earlywood vessel area of European oak (Quercus robur) in N-Poland. Palaeogeogr. Palaeoclimatol. Palaeoecol. 449, 520–530. https://doi.org/10.1016/j.palaeo.2016.02.046.

Rathgeber, C.B.K., 2017. Conifer tree-ring density inter-annual variability - anatomical, physiological and environmental determinants. New Phytol. 216, 621–625. https://doi.org/10.1111/nph.14763.

Reid, E., Wilson, R., 2020. Delta blue intensity vs. Maximum density: a case study using Pinus uncinata in the Pyrenees. Dendrochronologia 61, 125706. https://doi.org/10.1016/j.dendro.2020.125706.

Roden, J.S., Ehleringer, J.R., 1999. Hydrogen and oxygen isotope ratios of tree-ring cellulose for riparian trees grown long-term under hydroponically controlled environments. Oecologia 121, 467–477.

Roig, F.A., Siegwolf, R., Boninsegna, J.A., 2006. Stable oxygen isotopes (δ 18O) in Austrocedrus chilensis tree rings reflect climate variability in northwestern Patagonia. Argentina. Int. J. Biometeorol. 51, 97–105. https://doi.org/10.1007/s00484-006-0049-4.

Rydval, M., Larsson, L.-Å., McGlynn, L., Gunnarson, B.E., Loader, N.J., Young, G.H.F., Wilson, R., 2014. Blue intensity for dendroclimatology: should we have the blues? Experiments from Scotland. Dendrochronologia 32, 191–204. https://doi.org/10.1016/j.dendro.2014.04.003.

Schneider, C.A., Rasband, W.S., Eliceiri, K.W., 2012. NIH Image to ImageJ : 25 years of image analysis. Nat. Methods 9, 671–675. https://doi.org/10.1038/nmeth.2089.

Schneider, L., Smerdon, J.E., Büntgen, U., Wilson, R.J.S., Myglan, V.S., Kirdyanov, A.V., Esper, J., 2015. Revising midlatitude summer temperatures back to A.D. 600 based on a wood density network. Geophys. Res. Lett. 42, 4556–4562. https://doi.org/10.1002/2015GL063956.

Schulman, E., 1956. Dendroclimatic Changes in Semiarid America. Arizona Press, Tucson.

Schweingruber, F.H., 1988. II Analysis of the materials. Tree rings: Basics and applications ofdendrochronology. Kluwer Academic Publishers. https://doi.org/10.1007/978-94-009-1273-1.

Scott, L., Manzano, S., Carr, A.S., Cordova, C., Ochando, J., Bateman, M.D., Carrión, J.S., 2021. A 14000 year multi-proxy alluvial record of ecotone changes in a Fynbos-Succulent Karoo transition in South Africa. Palaeogeogr. Palaeoclimatol. Palaeoecol. 569 https://doi.org/10.1016/j.palaeo.2021.110331.

St. George, S., Esper, J., 2018. Concord and discord among Northern Hemisphere paleotemperature reconstructions from tree rings. Quat. Sci. Rev. 13–16 https://doi.org/S0277379118307170.

Stager, J.C., Mayewski, P.A., White, J., Chase, B.M., Neumann, F.H., Meadows, M.E., King, C.D., Dixon, D.A., 2012. Precipitation variability in the winter rainfall zone of South Africa during the last 1400 yr linked to the austral westerlies. Clim. Past Discuss. 8, 877–887. https://doi.org/10.5194/cp-8-877-2012.

Szejner, P., Wright, W.E., Belmecheri, S., Meko, D., Leavitt, S.W., Ehleringer, J.R., Monson, R.K., 2018. Disentangling seasonal and interannual legacies from inferred patterns of forest water and carbon cycling using tree-ring stable isotopes. Glob. Chang. Biol. 24, 5332–5347. https://doi.org/10.1111/gcb.14395.

Szymczak, S., Häusser, M., Garel, E., Santoni, S., Huneau, F., Knerr, I., Trachte, K., Bendix, J., Bräuning, A., 2020. How do mediterranean pine trees respond to drought and precipitation events along an elevation gradient? Forests 11, 758. https://doi.org/10.3390/f11070758.

Therrell, M.D., Stahle, D.W., Ries, L.P., Shugart, H.H., 2006. Tree-ring reconstructed rainfall variability in Zimbabwe. Clim. Dyn. 26, 677–685. https://doi.org/10.1007/s00382-005-0108-2.

Trouet, V., Van Oldenborgh, G.J., 2013. KNMI climate explorer: a web-based research tool for high-resolution paleoclimatology. Tree-Ring Res. 69, 3–13. https://doi.org/10.3959/1536-1098-69.1.3.

Treydte, K.S., Schleser, G.H., Helle, G., Frank, D.C., Winiger, M., Haug, G.H., Esper, J., 2006. The twentieth century was the wettest period in northern Pakistan over the past millennium. Nature 440, 1179–1182. https://doi.org/10.1038/nature04743.

Trouet, V., Esper, J., Beeckman, H., 2010. Climate/growth relationships of Brachystegia spiciformis from the miombo woodland in south central Africa. Dendrochronologia 28, 161–171. https://doi.org/10.1016/j.dendro.2009.10.002.

Trouet, V., Panayotov, M.P., Ivanova, A., Frank, D., 2012. A pan-European summer teleconnection mode recorded by a new temperature reconstruction from the northeastern Mediterranean (ad 1768-2008). Holocene 22, 887–898. https://doi.org/10.1177/0959683611434225.

Tyson, P.D., Cooper, G.R.J., McCarthy, T.S., 2002. Millennial to multi-decadal variability in the climate of southern Africa. Int. J. Climatol. 22, 1105–1117. https://doi.org/10.1002/joc.787.

Valsecchi, V., Chase, B.M., Slingsby, J.A., Carr, A.S., Quick, L.J., Meadows, M.E., Cheddadi, R., Reimer, P.J., 2013. A high resolution 15,600-year pollen and microcharcoal record from the Cederberg Mountains, South Africa. Palaeogeogr. Palaeoclimatol. Palaeoecol. 387, 6–16. https://doi.org/10.1016/j.palaeo.2013.07.009.

Van den Bulcke, J., Wernersson, E.L.G., Dierick, M., Van Loo, D., Masschaele, B., Brabant, L., Boone, M.N., Van Hoorebeke, L., Haneca, K., Brun, A., Luengo Hendriks, C.L., Van Acker, J., 2014. 3D tree-ring analysis using helical X-ray tomography. Dendrochronologia 32, 39–46. https://doi.org/10.1016/j.dendro.2013.07.001.

Van den Bulcke, J., Boone, M.A., Dhaene, J., Van Loo, D., Van Hoorebeke, L., Boone, M. N., Wyffels, F., Beeckman, H., Van Acker, J., De Mil, T., 2019. Advanced X-ray CT scanning can boost tree-ring research for earth-system sciences. Ann. Bot. https://doi.org/10.1093/aob/mcz126.

Vlassenbroeck, J., Dierick, M., Masschaele, B., Cnudde, V., Van Hoorebeke, L., Jacobs, P., 2007. Software tools for quantification of X-ray microtomography at the UGCT. Nucl. Instruments Methods Phys. Res. Sect. A Accel. Spectrometers, Detect. Assoc. Equip. 580, 442–445. https://doi.org/10.1016/j.nima.2007.05.073.

Wolski, P., Conradie, S., Jack, C., Tadross, M., 2021. Spatio-temporal patterns of rainfall trends and the 2015–2017 drought over the winter rainfall region of South Africa. Int. J. Climatol. 41, E1303–E1319. https://doi.org/10.1002/joc.6768.

Woodborne, S., Hall, G., Jones, C.W., Loader, N.J., Patrut, A., Patrut, R.T., Robertson, I., Winkler, S.R., Winterbach, C.W., 2018. A 250-year isotopic proxy rainfall record from southern botswana. Stud. Univ. Babes-Bolyai Chem. 63, 109–124. https://doi.org/10.24193/subbchem.2018.1.09.

Zang, C., Biondi, F., 2014. Treeclim: an R package for the numerical calibration of proxy-climate relationships. Ecography (Cop.). 1–6. https://doi.org/10.1111/ecog.01335.

Zucchini, W., Hiemstra, L., 1983. A Note on the Relationship between Annual Rainfall and Tree Ring Indices for One Site in South Africa. Water SA 7600.

Zweifel, R., Häsler, R., 2001. Dynamics of water storage in mature subalpine Picea abies: temporal and spatial patterns of change in stem radius. Tree Physiol. 21, 561–569. https://doi.org/10.1093/treephys/21.9.561.